Probing *CPT* breaking induced by quantum decoherence at DUNE

J. C. Carrasco, F. N. Díaz, and A. M. Gago
Sección Física, Departamento de Ciencias, Pontificia Universidad Católica del Perú, Apartado 1761, Lima, Perú

(Received 18 December 2018; published 16 April 2019)

We show that the decoherence phenomena applied to the neutrino system could lead to an observable breaking of the fundamental *CPT* symmetry. We require specific textures of nondiagonal decoherence matrices, with nonzero δ_{CP}, for making such observations. Using the information from the *CPT* conjugate channels $\nu_\mu \to \nu_\mu$ and $\bar{\nu}_\mu \to \bar{\nu}_\mu$ and their corresponding backgrounds, we have estimated the sensitivity of the DUNE experiment for testing *CPT* under the previous conditions. Four scenarios for energy-dependent decoherence parameters, $\Gamma_{E_\nu} = \Gamma \times (E_\nu/\mathrm{GeV})^n$, $n = -1$, 0, 1, and 2, are taken into account, and for most of them, DUNE is able to achieve a 5σ discovery potential, having Γ in $\mathcal{O}(10^{-23}\ \mathrm{GeV})$ for $\delta_{CP} = 3\pi/2$. Meanwhile, for $\delta_{CP} = \pi/2$, we reach 3σ for Γ in $\mathcal{O}(10^{-24}\ \mathrm{GeV})$.

DOI: 10.1103/PhysRevD.99.075022

I. INTRODUCTION

Neutrino oscillation is provoked by the existence of nonzero neutrino masses allied with the mismatch between the corresponding eigenstates and the neutrino flavor eigenstates. This phenomenon is supported by overwhelming experimental evidence which spans more than two decades [1–10]. Notwithstanding neutrino oscillation being well established, the coexistence of new physics as a subleading effect of it has not been yet ruled out. In some occasions, this new physics brings about the option of breaking fundamental laws of nature—for instance, the violation of the equivalence principle [11–13] or the violation of Lorentz invariance [14–16]. The latter is described within the Lagrangian of the Standard Model extension (SME) [17], where one can find terms that explicitly violate the combined action of the conjugation (C), the parity-inversion (P), and the time-inversion (T) symmetries, known in short as the *CPT* symmetry. This combined symmetry holds for a local, Lorentz-invariant, and unitary quantum field theory. There has been a lot of work on testing *CPT* violation (CPTV) on the side of the SME [18–21]. We must remark that there is CPTV in the neutrino oscillation in matter, originated by the unequal number of particles and antiparticles in ordinary matter [22].

On the other hand, there is a set of theoretical hypotheses such as strings, branes [23,24], and quantum gravity [25], whose effects can be encoded behind an omnipresent environment that could be weakly interacting with neutrinos [26,27]. This type of interaction is written according to the open system formalism and has as a typical trait (in its simplistic version) the appearance of decoherence (damping) factors $\exp^{-\Gamma t}$ within the neutrino oscillation probabilities [28–35]. Here arises another type of CPTV rooted in the impossibility of defining a *CPT* operator by virtue of the evolution from pure states to mixed states, caused by decoherence [36,37]. In the open system approach, the effects of the environment are enclosed, in a model-independent way, in the so-called dissipative or decoherence matrix (after tracing out the environment's degrees of freedom). Thereby, it is uncertain to claim that this type of CPTV is genuine—i.e., that there is a fundamental arrow of time—or that it is only an apparent CPTV, in view of our lack of knowledge of the complete system. One way or another, an eventual observation of CPTV will shake our current understanding of fundamental physics.

In this paper, we will focus on different nondiagonal textures of the dissipative matrix, paying special attention to those which can produce an observable nonzero CPTV. An equal response of the environment for neutrinos and antineutrinos will be one of our working hypotheses. This stands in contrast to the hypothesis used, for instance, in Ref. [31]. We will also consider the possibility that the parameters of the dissipative matrix can be energy dependent [38,39]. We will use the DUNE experiment [40,41] as the scenario for assessing how significant a CPTV signature caused by quantum decoherence would be.

II. THEORETICAL APPROACH

A. Neutrino as open quantum system

Our aim is to treat the neutrino as a subsystem interacting, weakly, with a large (unknown) environment. In situations of

this kind, the linear evolution of the reduced density matrix of the subsystem is represented by means of the Lindblad master equation [26,27]:

$$\frac{\partial\rho(t)}{\partial t} = -i[H,\rho(t)] + \mathcal{D}[\rho(t)], \tag{1}$$

where $\rho(t)$ is the neutrino density matrix, H is the Hamiltonian of the neutrino subsystem, and $\mathcal{D}[\rho(t)]$ is the dissipative term where the decoherence phenomena is encoded. This dissipative factor is written as follows:

$$\mathcal{D}[\rho(t)] = \frac{1}{2}\sum_j([A_j,\rho(t)A_j^\dagger] + [A_j\rho(t),A_j^\dagger]). \tag{2}$$

Considering a three-level system, we can expand the operators in Eq. (1) in the basis of the Gell-Mann matrices from the $SU(3)$ group plus the identity matrix:

$$\rho = \sum \rho_\mu t_\mu, \quad H = \sum h_\mu t_\mu, \quad A_j = \sum a_\mu^j t_\mu, \tag{3}$$

where μ is running from 0 to 8, with t_0 being the identity matrix and t_k being the Gell-Mann matrices ($k = 1,\ldots,8$), which satisfy $[t_a,t_b] = i\sum_c f_{abc}t_c$, where f_{abc} are the structure constants of $SU(3)$. Imposing the von Neumman entropy, which increases with time, the Hermiticity of the $\hat{A}_j$ is assured, having, as a consequence, that the dissipative matrix can be expressed as [30]

$$D_{kj} = \frac{1}{2}\sum_{l,m,n}(a_{nl})f_{knm}f_{mlj}, \qquad a_{nl} = \vec{a}_n.\vec{a}_l, \tag{4}$$

with the matrix $\mathbf{D} \equiv D_{kj}$ being symmetric, with components $D_{\mu 0} = D_{0\mu} = 0$, and $\vec{a}_r = \{a_r^1, a_r^2, \ldots, a_r^8\}$. The complete positivity condition requires that the eigenvalues of the mixing matrix $\rho(t)$ be positive at any time; this is achieved by demanding that the matrix $\mathbf{A} \equiv a_{nl}$ be positive [26,27]. The scalar product structure present in the elements D_{kj} causes them to respect the Cauchy-Schwartz inequalities. Gathering the conservation of probability to all that we have said, we have that the evolution equation of $\rho(t)$ is given by

$$\dot{\rho}_0 = 0, \qquad \dot{\rho}_k = (H_{kj} + D_{kj})\rho_j = M_{kj}\rho_j, \tag{5}$$

where $H_{kj} = \sum_i h_i f_{ijk}$. The solution of Eq. (5) written in matricial form is

$$\varrho(t) = e^{\mathbf{M}t}\varrho(0), \tag{6}$$

where ϱ is an eight-column vector composed by ρ_k and $\mathbf{M} \equiv M_{kj}$. Therefore, we can obtain a general expression for the neutrino oscillation probability $\nu_\alpha \to \nu_\beta$:

$$P_{\nu_\alpha\to\nu_\beta} = \frac{1}{3} + \frac{1}{2}(\varrho^\beta)^T\varrho^\alpha(t) = \frac{1}{3} + \frac{1}{2}\sum_{i,j}\rho_i^\beta\rho_j^\alpha[e^{\mathbf{M}t}]_{ij}. \tag{7}$$

Since in our analytical approach we will use the vacuum case, the ρ_i^α's are already defined, and they are given by

$$\begin{aligned}
\rho_0^\alpha &= \sqrt{2/3},\\
\rho_1^\alpha &= 2\,\mathrm{Re}(U_{\alpha1}^*U_{\alpha2}),\\
\rho_2^\alpha &= -2\,\mathrm{Im}(U_{\alpha1}^*U_{\alpha2}),\\
\rho_3^\alpha &= |U_{\alpha1}|^2 - |U_{\alpha2}|^2,\\
\rho_4^\alpha &= 2\,\mathrm{Re}(U_{\alpha1}^*U_{\alpha3}),\\
\rho_5^\alpha &= -2\,\mathrm{Im}(U_{\alpha1}^*U_{\alpha3}),\\
\rho_6^\alpha &= 2\,\mathrm{Re}(U_{\alpha2}^*U_{\alpha3}),\\
\rho_7^\alpha &= -2\,\mathrm{Im}(U_{\alpha2}^*U_{\alpha3}),\\
\rho_8^\alpha &= \frac{1}{\sqrt{3}}(|U_{\alpha1}|^2 + |U_{\alpha2}|^2 - 2|U_{\alpha3}|^2),
\end{aligned} \tag{8}$$

where $U_{\alpha j}$ refers to an element of the Pontecorvo-Maki-Nakagawa-Sakata (PMNS) matrix [42,43]. If we want to solve Eq. (7) for the antineutrino case, it is enough to make $U_{\alpha j} \to U_{\alpha j}^*$.

B. *CPT* violation and quantum decoherence

We will test the *CPT* symmetry in the context of DUNE using the simulated total rates associated with the ν_μ and the $\bar{\nu}_\mu$ survival channels, where the matter effects are unimportant. The latter fact implies that the vacuum probability formulas for oscillation (plus decoherence) are going to be sufficient for understanding the corresponding features of CPTV effects. Thus, all the formulas in this section will be developed under the vacuum framework. Before starting, it is of the utmost importance to remark that the decoherence phenomena entails the transition from pure to mixed states, which implies that the time-reversal operation is, as itself, meaningless for this situation [36]. The tool for revealing these implicit CPTV effects is the difference between the ν_μ and $\bar{\nu}_\mu$ survival probability channels, which, written for a generic flavor ν_α, is

$$\Delta P_{\not{CPT}} = P_{\nu_\alpha\to\nu_\alpha} - P_{\bar{\nu}_\alpha\to\bar{\nu}_\alpha}. \tag{9}$$

With the aim of simplifying the analytical form of the latter expression, we work under three assumptions: that the diagonal elements (damping parameters) of the dissipative matrix $\mathbf{D}$ are all equal to a single parameter Γ; that the dissipative matrix for neutrinos is equal to the corresponding for antineutrinos, $\mathbf{D} = \bar{\mathbf{D}}$; and that the $\mathbf{D}$ matrix contains no more than one nondiagonal element at the time we study the $\Delta P_{\not{CPT}}$. As a general feature, we have that a nonzero $\Delta P_{\not{CPT}}$ is obtained when in the survival neutrino

oscillation probability there is a term with β_{ij} (nondiagonal term) coupled to $\rho_i^\alpha \rho_j^\alpha$ that contains $\sin\delta_{CP}$; therefore, when its corresponding antineutrino term is subtracted in order to get $\Delta P_{\not CPT}$, they do not cancel each other because of the flipping of the sign of $\sin\delta_{CP}$. We find that the aforementioned situation (i.e., non-null $\Delta P_{\not CPT}$) is fulfilled by 15 β_{ij}'s: those where one coefficient in the product $\rho_i^\alpha \rho_j^\alpha$ is ρ_2^α, ρ_5^α, or ρ_7^α, and the other one is ρ_1^α, ρ_3^α, ρ_4^α, ρ_6^α, or ρ_8^α, summarizing in total 15 cases. The remaining β_{ij}'s do not produce non-null $\Delta P_{\not CPT}$, given that they are not connected with $\rho_i^\alpha \rho_j^\alpha$ terms that contain $\sin\delta_{CP}$, similar to what happens for the survival probabilities; in the pure oscillation case, where there are no terms involving $\sin\delta_{CP}$, these do not flip sign when we switch neutrinos to antineutrinos, conserving *CPT*.

Based on the similarities of the structure of the form for $\Delta P_{\not CPT}$, we can divide these 15 cases into two groups, each group related to different set of β_{ij}'s, which we present as follows.

1. $\Delta P_{\not CPT}$ for group 1

The $\Delta P_{\not CPT}$ expression for the first group is given by

$$\Delta P_{\not CPT} = \beta_{ij} \frac{(e^{\Omega_{\beta_{ij}} t} - e^{-\Omega_{\beta_{ij}} t})}{\Omega_{\beta_{ij}}} \rho_i^\alpha \rho_j^\alpha e^{-\Gamma t}, \qquad (10)$$

where $\Omega_{\beta_{ij}} = \sqrt{\beta_{ij}^2 - \Delta_{\beta_{ij}}{}^2}$, with $\Delta_{\beta_{ij}} = \Delta m^2_{\beta_{ij}}/2E$, where E is energy and $\Delta m^2_{\beta_{ij}}$ corresponds to standard mass-squared differences of neutrino masses, according to its indices ij (see Table I). This formula applies for nine β_{ij}'s, and the details are given in Table I. On the other hand, in Appendix A, as an example, we display in Eq. (A2) the exact probability from which we can extrapolate the $\Delta P_{\not CPT}$ for β_{12}.

2. $\Delta P_{\not CPT}$ for group 2

The $\Delta P_{\not CPT}$ for the remaining six β_{ij}'s—β_{15}, β_{24}, β_{17}, β_{26}, β_{47}, and β_{56}—is also proportional to β_{ij}, but it is rather a cumbersome expression in comparison to the one in Eq. (10). In fact, it is the addition of two terms, one of them proportional to $\rho_i^\alpha \rho_j^\alpha$, and the other proportional to $\rho_k^\alpha \rho_l^\alpha$. For a given set of ij indices, there is a specific kl, with each one of these indices associated with an specific mass-squared difference value; for the complete details, see Table II. The six expressions for the CPTV formula are obtained per each pair ij, kl plus exchanging $ij \leftrightarrow kl$, with all the correspondent terms associated with them. The explicit formula is given by

$$\Delta P_{\not CPT} = \beta_{ij} \frac{1}{\sqrt{\Omega^4 - 4\Delta^2_{\beta_{ij}} \Delta^2_{\beta_{kl}}}} \times \left[(\Omega_+ (e^{\Omega_+ t} - e^{-\Omega_+ t}) - \Omega_- (e^{\Omega_- t} - e^{-\Omega_- t})) \rho_i^\alpha \rho_j^\alpha + \Delta_{\beta_{ij}} \Delta_{\beta_{kl}} \left(\frac{e^{\Omega_+ t} - e^{-\Omega_+ t}}{\Omega_+} - \frac{e^{\Omega_- t} - e^{-\Omega_- t}}{\Omega_-} \right) \rho_k^\alpha \rho_l^\alpha \right] e^{-\Gamma t}, \qquad (11)$$

where $\Omega^2 = \beta_{ij}^2 - \Delta^2_{\beta_{ij}} - \Delta^2_{\beta_{kl}}$ and $\Omega_\pm = \frac{1}{\sqrt{2}} \times \sqrt{\Omega^2 \pm \sqrt{\Omega^4 - 4\Delta^2_{\beta_{ij}} \Delta^2_{\beta_{kl}}}}$. As in the case of group 1, the probability for β_{24} is shown in Appendix A in Eq. (A3). From there, the corresponding $\Delta P_{\not CPT}$ can be extracted.

3. $\Delta P_{\not CPT}$ analytical results

It is important to point out that from now on, in all the results that we will present, $\Delta P_{\not CPT}$ will be calculated for $\alpha = \mu$. In Fig. 1, we present $\Delta P_{\not CPT}$ in two separated plots:

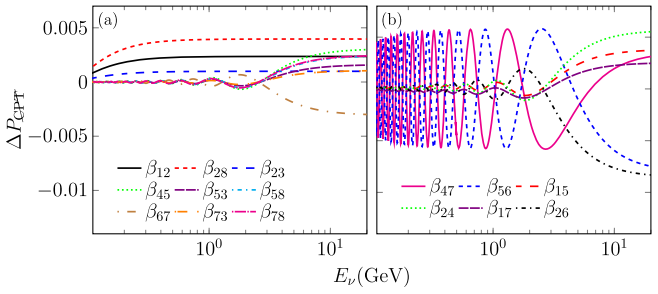

FIG. 1. $\Delta P_{\not CPT}$ vs E_ν, evaluated for $\Gamma = 10^{-23}$ GeV and $\delta_{CP} = 3\pi/2$. (a) Group 1 with β_{28}, β_{53}, $\beta_{73} = \Gamma/\sqrt{3}$, β_{58}, $\beta_{78} = \Gamma/\sqrt{7}$, β_{12}, β_{23}, β_{45}, $\beta_{67} = \Gamma/3$. (b) Group 2 with all β's equal to $\Gamma/\sqrt{3}$. The remaining parameters are given in Table III.

TABLE I. Each group of indices (i, j) that corresponds to one of the nine β_{ij}'s. The (i, j)'s in the same row are associated with the $\Delta_{\beta_{ij}}$ in the right column of the same line.

(i, j)	$\Delta_{\beta_{ij}}$
(1, 2), (2, 3), (2, 8)	Δ_{12}
(4, 5), (5, 3), (5, 8)	Δ_{13}
(6, 7), (7, 3), (7, 8)	Δ_{23}

TABLE II. The relations between the six indices (i, j) and (k, l), each of them associated with its corresponding β and its neutrino mass-squared differences.

$\{(i,j), \Delta_{\beta_{ij}}\} \leftrightarrow \{(k,l), \Delta_{\beta_{kl}}\}$
$\{(1,5), \Delta_{12}\} \leftrightarrow \{(2,4), \Delta_{13}\}$
$\{(1,7), \Delta_{12}\} \leftrightarrow \{(2,6), \Delta_{23}\}$
$\{(4,7), \Delta_{13}\} \leftrightarrow \{(5,6), \Delta_{23}\}$

TABLE III. DUNE baseline and values for standard oscillation parameters taken from Ref. [44].

Parameter	Value
θ_{12}	33.63°
θ_{13}(NH)	8.52°
θ_{23}(NH)	48.7°
Δm^2_{21}	7.4×10^{-5} eV^2
Δm^2_{31}(NH)	2.515×10^{-3} eV^2
Baseline	1300 km

all β's for group 1 and group 2, for neutrino energies from 0.1 to 20 GeV, which encloses the DUNE energy range. We have evaluated this effect in an isolated manner per each β (i.e., considering all the rest of the β's to be zero), considering its maximum value, which is obtained from the inequalities and positivity conditions given in Appendix B, having the following results: β_{28}, β_{53}, $\beta_{73} = \Gamma/\sqrt{3}$, β_{58}, $\beta_{78} = \Gamma/\sqrt{7}$, β_{12}, β_{23}, β_{45}, $\beta_{67} = \Gamma/3$, and the remaining β's with $\Gamma/\sqrt{3}$, where we have taken their positive values. For all these plots, it is also fixed that $\delta_{CP} = 3\pi/2$ and $\Gamma = 10^{-23}$ GeV, and the remaining parameters are displayed in Table III. The parameters given in Table III will be used throughout this paper. We note for group 1 that β_{28} is producing the highest amplitude for $\Delta P_{\not{CPT}}$ in the entire energy range, with β_{12} being second. In the case of group 2, β_{47} and β_{56} give the maximum values of amplitudes of $\Delta P_{\not{CPT}}$ up to neutrino energies a bit less than 5 GeV.

In Fig. 2, we have four plots which show isocontour curves of $\Delta P_{\not{CPT}}$ at the plane Γ vs δ_{CP}: two of them correspond to the vacuum oscillation case (top), and the other two to the matter oscillation case (bottom). For all plots, the neutrino energy is fixed at 2.4 GeV, keeping the remaining parameters at the same values as those used for Fig. 1. Two plots are for β_{28} (group 1) for vacuum and matter, and the corresponding other two are for β_{56} (group 2). All β's are equal to $\Gamma/\sqrt{3}$. We have chosen these particular β's since they are the ones that generate the biggest amplitudes for $\Delta P_{\not{CPT}}$ for each group. Among the general features, we have that other than the maximum (and minimum) value of the $\Delta P_{\not{CPT}}$, the behavior of all plots is rather equal. Another common detail is that $\Delta P_{\not{CPT}}$ grows with Γ until reaching a region where the maximum amplitude is located, and then starts to decrease. Outside the regions around the peaks, i.e., for lower and higher values than the Γ at the peak, the $\Delta P_{\not{CPT}}$ is zero. The vacuum and the matter case exhibit a very similar pattern, and there is not a qualitative difference between the plots for β_{28} (group 1) and β_{56} (group 2). Therefore, to get a full understanding of what happens, we can use the vacuum formula given for group 1 in Eq. (10). Hence, from Eq. (10), we see that $\Delta P_{\not{CPT}}$ is suppressed for low values

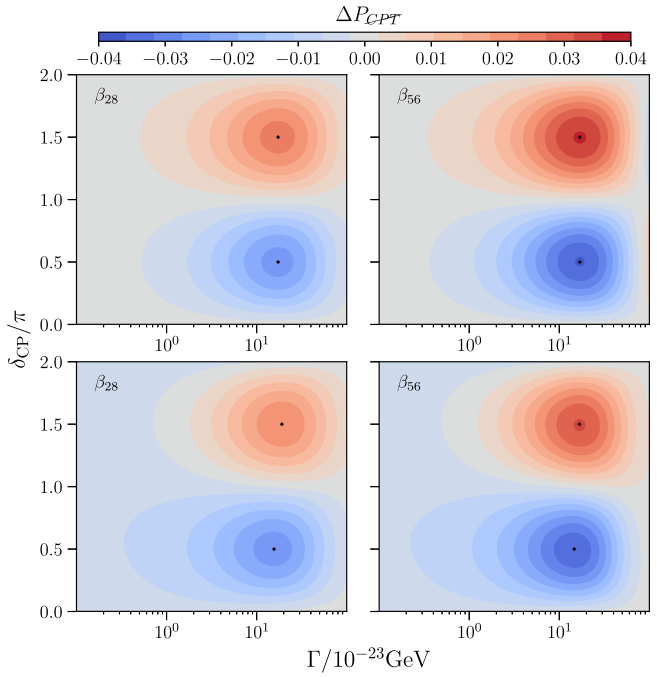

FIG. 2. Isocontour curves of $\Delta P_{\not{CPT}}$ at the plane Γ vs δ_{CP} evaluated for $\beta_{28} = \Gamma/\sqrt{3}$ and $\beta_{56} = \Gamma/\sqrt{3}$ and for a fixed $E_\nu = 2.4$ GeV. The two plots at the top correspond to the vacuum oscillation case, while the two plots at the bottom correspond to the matter oscillation case.

of Γ, which implies low values of $\beta_{28}(= \Gamma/\sqrt{3})$ that are directly proportional to the value of $\Delta P_{\not{CPT}}$. On the other hand, $\Delta P_{\not{CPT}}$ is reduced for higher values of Γ, given that the latter diminishes the factor $\exp^{-\Gamma t}$. From the maximization of the Eq. (10), the value of Γ at the peak can be extracted: for β_{28}, the peak is at $\Gamma \sim 1.7 \times 10^{-22}$ GeV. Similarly, if we maximize Eq. (11), we obtain the peak for β_{56} at $\Gamma \sim 1.6 \times 10^{-22}$ GeV. In general, a very reasonable estimation for the value of Γ at the peak is obtained from $\Gamma L \sim 1$ (and then $\Gamma \sim 1/L$), which for $L = 1300$ km gives $\sim 1.5 \times 10^{-22}$ GeV. The corresponding values of $\delta_{CP} = \pi/2$ and $3\pi/2$, for β_{28}, can be directly inferred from the unique presence of $\sin\delta_{CP}$ in the factor $\rho^\mu_2 \rho^\mu_8$; the values of δ_{CP} for β_{56} are very close to $\pi/2$ and $3\pi/2$ for similar reasons, but they are slightly distorted due to ρ^μ_6 being composed by two terms, with one of them proportional to $\cos\delta_{CP}$. In spite of this, the vacuum and matter cases look nearly alike. We must note that the matter effects produce a $\Delta P_{\not{CPT}} \neq 0$ even in the absence of decoherence. Actually, in the experimental (simulated) searches of CPTV that we will present in the following sections, the CPTV, due to matter effects, will play the role of normalization factor.

4. Decoherence parameters with energy dependency

From a more general view, the entries of the decoherence matrix could be energy dependent; particularly, in this paper, we will adopt this dependence as follows:

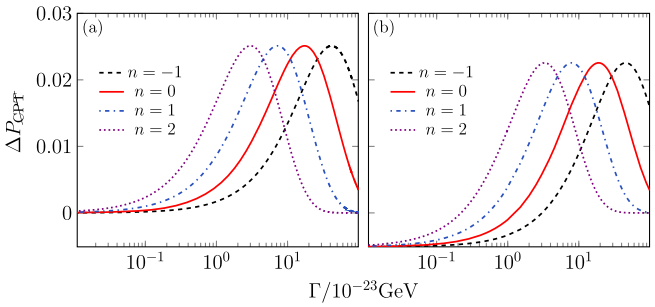

FIG. 3. $\Delta P_{\not CPT}$ vs Γ, evaluated for different energy dependences $n=-1$, 0, 1, 2; $E_\nu = 2.4$ GeV; $\delta_{CP} = 3\pi/2$; and fixing $\beta_{28} = \Gamma/\sqrt{3}$. We have (a) the vacuum oscillation case, and (b) the matter oscillation case. In both plots we use the same scale.

$$\Gamma_{E_\nu} = \Gamma\left(\frac{E_\nu}{\mathrm{GeV}}\right)^n, \tag{12}$$

where n can be -1, 0, 1, or 2. The value $n=-1$ is taken because it imitates the oscillation energy dependence, while the motivation for $n=1$ and $n=2$ can be found in Refs. [38,39], respectively.

In Fig. 3, we study $\Delta P_{\not CPT}$ for the aforementioned energy dependences, and we set $\beta_{28} = \Gamma/\sqrt{3}$, the neutrino energy in 2.4 GeV (the DUNE energy peak) and $\delta_{CP} = 3\pi/2$, for both the vacuum and matter oscillation cases. In these figures, we note that the energy's dependency on Γ only changes their values at the peak but does not affect the amplitude of $\Delta P_{\not CPT}$. As we have discussed in Sec. II B 3, the value at the peak satisfies approximately the relation $\Gamma_{E_\nu} L \sim 1$, and then $\Gamma \sim 1/(LE^n)$, which turns out to be $\Gamma \sim \{4.0, 1.5, 0.6, 0.3\} \times 10^{-22}$ GeV for $n=-1$, 0, 1, and 2, respectively. As expected, we have a non-negligible negative value of $\Delta P_{\not CPT}$ when Γ goes to zero for the matter oscillation case.

5. Optimal $\Delta P_{\not CPT}$

For maximizing $\Delta P_{\not CPT}$, we simultaneously turn on β_{28}, β_{12}, β_{56}, and β_{47} with the following values: $\beta_{28} = \Gamma/\sqrt{3}$, $\beta_{12} = (\sqrt{2/3})\Gamma/3$, and $\beta_{56} = -\beta_{47} = \Gamma/3$. These values has been set according to the following steps: First, we fix $\beta_{28} = \Gamma/\sqrt{3}$, given that this β produces the major effect on $\Delta P_{\not CPT}$. Second, once β_{28} has been defined, we obtain the maximum allowed value for β_{12}, which is second in importance regarding its impact on $\Delta P_{\not CPT}$. Finally, with β_{28} and β_{12} already set up, we get the maximum values of β_{56} and β_{47}, where we take $\beta_{56} = -\beta_{47}$ in order to obtain a constructive effect between them. The restrictions imposed by the Schwarz inequalities and positivity conditions, fully described in Appendix B, have been considered in getting the aforementioned values of the β's.

6. CPT violation in matter

As we have already mentioned, when the neutrinos are traveling through matter, we have a nonzero CPTV value for pure standard oscillation, even for zero CP phase. From now on, when we refer to the term standard oscillation (SO), it means that the matter effects are included. If we add the decoherence to SO, the nonzero value of CPTV is still preserved, but it has a different magnitude with respect to its corresponding value in the pure SO, because, as expected, it is distorted by the presence of the quantum decoherence parameters. In particular, it is interesting to note that this happens even when a single-parameter diagonal decoherence matrix (DDM) (proportional to the identity) is considered, in contrast with the DDM case in vacuum, where a nonzero CPTV is not brought to light. The matter neutrino oscillation probabilities for a single-parameter DDM can be derived only by replacing the vacuum mixing angles and mass squared with the corresponding ones in matter—in, for instance, the three-generation formula displayed in Ref. [30]. Of course, this also includes the replacement of a singular decoherence parameter. The application of the latter procedure is fully justified and has been very well explained in Ref. [35]. Therefore, we have that the structure of the formula is given by

$$P^{\mathrm{SO}\oplus\mathrm{DDM}}_{\nu_\alpha\nu_\rho} = \frac{1}{3}(1-e^{-\Gamma t}) + e^{-\Gamma t} P^{\mathrm{SO}}_{\nu_\alpha\nu_\rho}, \tag{13}$$

where α, ρ are neutrino flavours, and SO(SO $\oplus$ DDM) stands for standard oscillation (standard oscillation plus diagonal decoherence). It is clear that $\Delta P^{\mathrm{SO}\oplus\mathrm{DDM}}_{\not CPT} = e^{-\Gamma t}\Delta P^{\mathrm{SO}}_{\not CPT}$, which goes to zero for high values of Γ. Nonetheless, when we deal with a real situation, the latter does not occur, since we have to convolute the neutrino (antineutrino) oscillation probabilities with the neutrino (antineutrino) fluxes, cross sections, efficiencies, and resolution, being that, for this context, the $1/3$ from the first term on the rhs in Eq. (13) is the only one that survives for high values of Γ, leading us to find a nonzero constant value. We will see this type of behavior further ahead in our results section.

In this paper, we are not going to derive analytical formulas for the neutrino matter oscillation probabilities of the nondiagonal decoherence matrix (NDM) cases that we have presented before. This is because it is a rather complicated task, and besides, as we have already argued, the vacuum oscillation probability formulas are going to be enough to give us a qualitative understanding of our results.

III. EXPERIMENT, SIMULATION, AND RESULTS

The DUNE experiment will be able to unravel several nonstandard neutrino physics scenarios through oscillation

measurements [45–47]. It will consist of a muon neutrino (antineutrino) beam traversing the Earth from Fermilab to Sanford Underground Research Facility (SURF), which comprises a distance of 1300 km and an average matter density of $\rho_{\mathrm{DUNE}} = 2.96\ \mathrm{g/cm^3}$. At SURF, the neutrino beam will hit a massive liquid argon time-projection chamber (LArTPC) of 40 Ktons [40].

For this work, it is assumed that the configuration used is 80 GeV energy with 1.07 MW power in the primary proton beam from the main injector running over 5 years for exposure for each mode, the forward horn current (FHC) and the reverse horn current (RHC). In our simulation of DUNE, the GLoBES package [48,49] is used, and it is fed with the information of the cross section, neutrino fluxes, resolution function, and efficiency extracted from Ref. [41]. Meanwhile, the matter neutrino oscillation probabilities plus decoherence was calculated with nuSQuIDS [50].

For testing the CPTV effects, the following experimental observable is defined:

$$\mathcal{R} = \frac{\Delta N^{\mathrm{SO}\oplus\mathrm{DEC}}}{\Delta N^{\mathrm{SO}}}, \tag{14}$$

where $\Delta N^{\mathrm{SO(SO}\oplus\mathrm{DEC)}} = N_{\nu_\mu} - N_{\bar{\nu}_\mu}$ is the difference between the total event rates for neutrinos and antineutrinos, respectively, and DEC stands for any case of decoherence.

The total event rates have been calculated using the prescription given in Ref. [40], where the signal is composed of $\nu_\mu + \bar{\nu}_\mu$ charge current event rates, while the background is composed of neutral current event rates and the $\nu_\tau + \bar{\nu}_\tau$ charge current event rates. Our observable is normalized with the SO difference of events ΔN^{SO}, which is nonzero due to matter effects plus the intrinsic differences between the cross sections, fluxes, etc., for neutrinos and antineutrinos. Given our definition, when decoherence is absent, $\mathcal{R} = 1$.

To give an idea of the impact of decoherence on SO physics, we display in Table IV the total rates for four energy-dependent decoherence scenarios. We are not considering within this table the tau contamination [51,52], since this contribution is negligible.

TABLE IV. Total rates for the signals of ν_μ and $\bar{\nu}_\mu$ disappearance channels and their corresponding background. We consider $\delta_{CP} = 3\pi/2$.

$\Gamma = 10^{-23}$ GeV	Std	$n=-1$	$n=0$	$n=1$	$n=2$
Neutrino mode					
$\nu_\mu + \bar{\nu}_\mu$ CC signal	11749	11841	11965	11573	11932
NC background	109	109	109	109	109
$\nu_\tau + \bar{\nu}_\tau$ CC background	43	43	46	74	87
Antineutrino mode					
$\bar{\nu}_\mu + \nu_\mu$ CC signal	5903	5897	5846	5237	4816
NC background	58	58	58	58	58
$\nu_\tau + \bar{\nu}_\tau$ CC background	27	27	29	50	60

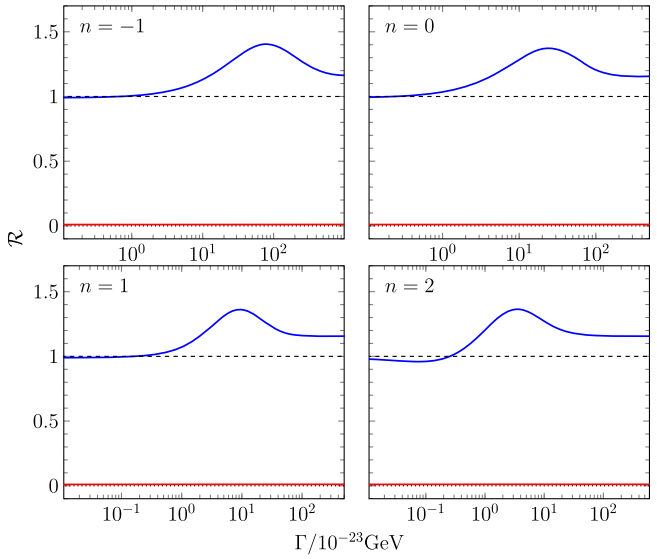

FIG. 4. Here we display $\mathcal{R}$ vs Γ for the four energy dependences $n = -1$, 0, 1, and 2, showing the signal (blue) and background (red). We consider $\delta_{CP} = 3\pi/2$.

Using the values of this table, we display in Fig. 4 the evaluation of $\mathcal{R}$ for the signal and background event rates, separately. We clearly see that the size of $\mathcal{R}$ for the backgrounds is very small in comparison with the corresponding one for the signal.

We also display in Fig. 5 two plots: θ_{23} vs θ_{12} and θ_{23} vs θ_{13}, varying the mixing angles within the 3σ range, showing the percentual variation of $\mathcal{R}$ ($\Delta\mathcal{R}\%$) with respect to the value obtained for the best-fit oscillation parameters

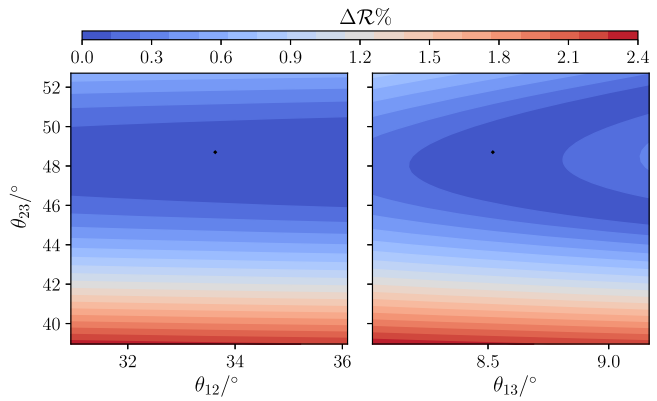

FIG. 5. Here we have two plots: θ_{23} vs θ_{12} and θ_{23} vs θ_{13}, varying the mixing angles within the 3σ range, showing the percentual variation of $\mathcal{R}$ with respect to the value obtained for the best-fit oscillation parameters given in Table III. The mixing angle that does not appear in the corresponding plot is fixed at its best-fit value. In all the plots, we fix $\Gamma = 10^{-23}$ GeV and $\delta_{CP} = 3\pi/2$.

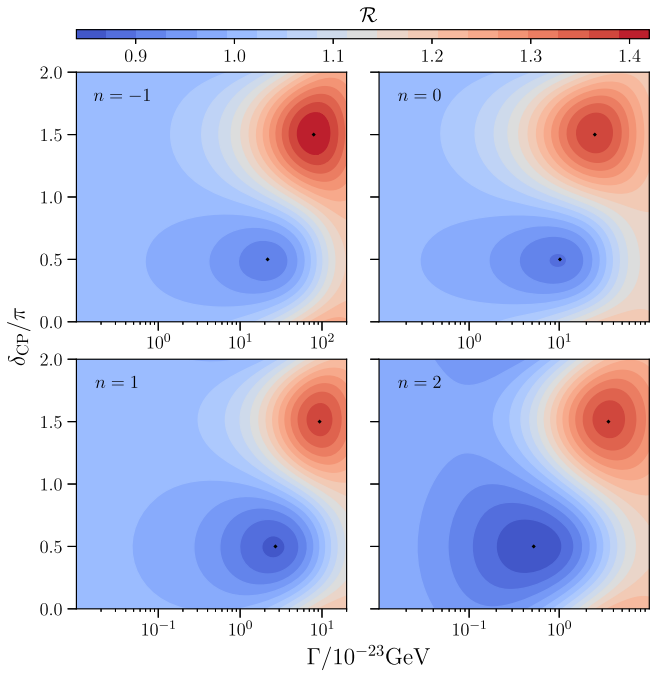

FIG. 6. We analyze the confidence levels for the maximum values for $\mathcal{R}$. For $\delta_{\rm CP} \sim \pi/2$ we have 2.9σ, 3.4σ, 4.7σ, and 5.5σ of confidence for $n = -1$, 0, 1, and 2, respectively. On the other hand, for $\delta_{\rm CP} \sim 3\pi/2$ we have 10.3σ, 9.8σ, 9.6σ, and 9.7σ of confidence for $n = -1$, 0, 1 and 2, respectively.

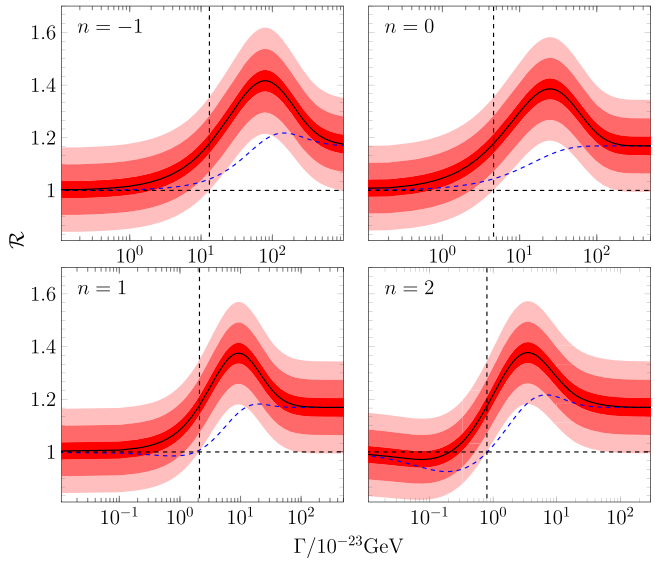

FIG. 7. The black horizontal dashed line is the expected value in the SO. The blue dashed line corresponds to the case of a DDM. Meanwhile, the solid black line corresponds to the case of a NDM, with both cases evaluated at $\delta_{CP} = 3\pi/2$. The red fringes (small, medium, and large) represent the statistical error for 1σ, 3σ, and 5σ (respectively). The β's used correspond to the ones given in Sec. II B 5. The intersection between the black horizontal dashed line and the vertical one marks the 5σ significance of the NDM case relative to the SO case.

given in Table III for $\Gamma = 10^{-23}$ GeV and $\delta_{CP} = 3\pi/2$. We observe in the two plots that the $\Delta\mathcal{R}\%$ varies at maximum ∼2.3%. We do not display the case of θ_{13} vs θ_{12} since the variation is much lower.

In Fig. 6, we show isocontour curves for the observable $\mathcal{R}$ in the plane Γ vs δ for four plots, which correspond to $n = -1$, 0, 1, and 2. In these plots, the maximum amplitudes are located at similar δ_{CP}, $\delta_{CP} \simeq \pi/2$, and $3\pi/2$ to those presented in Fig. 2. In relation to Fig. 2, there is a dislocation between the values of Γ at the maximum amplitudes for $\delta_{CP} \simeq \pi/2$ and $3\pi/2$. This is mainly because of the differences in the inputs used when we convolute the probabilities for the neutrino and antineutrino modes. In addition, the Γ for $\delta_{CP} \simeq \pi/2$ and $3\pi/2$ is shifted to lower values whenever n increases, gaining more sensitivity to lower values of Γ. This latter behavior is expected and resembles what we have seen for $\Delta P_{\not{CPT}}$ in Fig. 3 (but here is a one-dimensional view). Moreover, we also see the existence of degeneracies in (Γ, δ) like those we have seen in Ref. [35].

In Fig. 7, we present the observable $\mathcal{R}$, with its corresponding error bands for 1σ, 3σ, and 5σ, vs Γ, for $n = -1$, 0, 1, and 2. We take $\delta_{CP} = 3\pi/2$, given that we learn from Fig. 6 that one of the maximum amplitudes of $\Delta P_{\not{CPT}}$ is obtained at this δ_{CP}. The behavior displayed in this plot for small and medium values of Γ, at the given scale, is rather similar to that observed in Fig. 3. However, for large values of Γ, the observable $\mathcal{R} \sim 1.17$, and not ∼1.0, since within the signal for ν_μ ($\bar{\nu}_\mu$) we are including $\bar{\nu}_\mu(\nu_\mu)$ with their different fluxes and cross sections. Therefore, the link between these plots and those from Fig. 3 is not transparent. In order to make a comparison, we introduce in this plot the $\mathcal{R}$ corresponding to the single parameter DDM. We see that at small and large values of Γ, $\mathcal{R}$ tends to be ∼1 and ∼1.17 for the DDM and NDM, respectively, regardless of the dependency on n, as well. As we have anticipated in Sec. II B 6, the diagonal case also produces nonzero $\Delta P_{\not{CPT}}$, but with a lower magnitude than the NDM case. In fact, we have that for the NDM case a 5σ discrepancy, with respect to the expectation value for SO ($\mathcal{R} = 1$), is reached at $\Gamma = \{13.1, 4.6, 2.1, 0.8\} \times 10^{-23}$ GeV for $n = -1$, 0, 1, and 2, respectively. It is interesting to note that at these values of Γ, the DDM is compatible with the SO prediction. Thus, here we would be able to distinguish the NDM from the DDM.

An analogous result is shown in Fig. 8, but taking $\delta_{CP} = \pi/2$. In this case, the following values of Γ achieve 3σ significance: $\{21.6, 6, 0.8, 0.09\} \times 10^{-23}$ GeV for $n = -1$, 0, 1, and 2, respectively. All of them have $\mathcal{R} < 1$. For the cases $n = -1$, 0, we can discriminate between the NDM and DDM, since we have $\mathcal{R} < 1$ and $\mathcal{R} > 1$, respectively. For $n = 1$, the DDM case is congruent with the SO; meanwhile, for $n = 2$, the DDM and NDM can be confused.

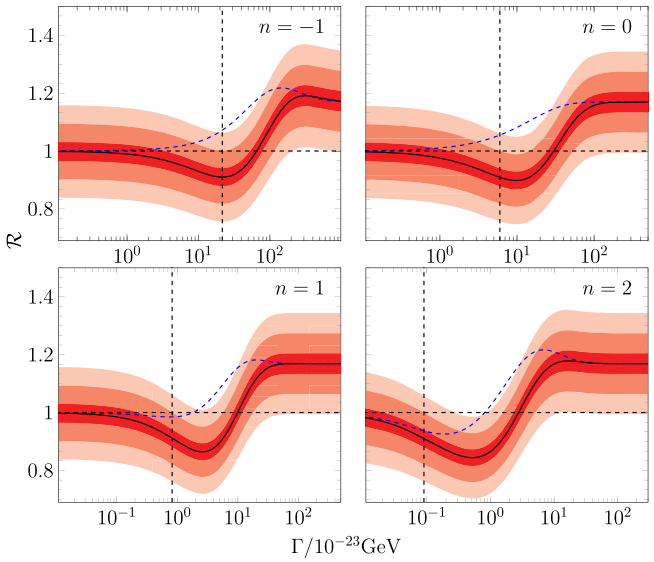

FIG. 8. Similar to Fig. 7, but for $\delta_{CP}=\pi/2$. Here, the intersection between the black horizontal dashed line and the vertical one marks the 3σ significance of the NDM case relative to the SO case.

IV. SUMMARY AND CONCLUSIONS

We have shown that an apparent breakdown of the fundamental *CPT* symmetry can take place when the neutrino system is affected by the environment. This CPTV is produced by the combination of having δ_{CP} in the neutrino sector with a certain set of some non-null coherence terms in the dissipative matrix. Furthermore, we have quantified a possible measurement of this CPTV using the disappearance channels $\nu_\mu \to \nu_\mu$ and $\bar{\nu}_\mu \to \bar{\nu}_\mu$, with their corresponding backgrounds, and an observable $\mathcal{R}$, all in the context of the DUNE experiment. The simulated measurements of $\mathcal{R}$ have been performed considering four hypothesis of energy dependence on the decoherence parameters: $n=-1$, 0, 1, and 2, where $\Gamma_{E_\nu}=\Gamma(E_\nu/\mathrm{GeV})^n$. For $\delta_{CP}=3\pi/2$, which is rather close to the current value of δ_{CP} given by the global fit [44], and a NDM, we achieve a significance of 5σ for $\mathcal{R}$ with respect to its expectation value at the SO case, $\mathcal{R}=1$, for the following Γ: $\{13.1, 4.6, 2.1, 0.8\}\times 10^{-23}$ GeV, for $n=-1$, 0, 1, and 2, respectively. At all these points, the DDM is compatible with the SO case. For $\delta_{CP}=\pi/2$, we reach discrepancies of the order of 3σ. In our best case for $n=2$ we have $\Gamma\simeq 10^{-24}$ GeV, but with the inability to discriminate from the DDM case. We have to keep in mind that the aforementioned observations of CPTV appear when the neutrino system is treated as an open system. This means that it is likely that if we had access to the information of the environment—i.e., to the whole system—the overall *CPT* symmetry would be conserved. For this reason, it requires a more profound discussion to ascertain if this CPTV is a breaking at the fundamental level or if it is only an apparent one, because of our lack of information from the environment. In some way, this CPTV represents a loss of information such that in order to show that this information is not destroyed, we need to know how this CPTV is compensated with the environment, by probing the conservation of the information.

ACKNOWLEDGMENTS

A. M. G. acknowledges funding by *the Dirección de Gestión de la Investigación* at Pontificia Universidad Católica del Perú, through Grant 494 No. DGI-2017-3-0019. J. C. C. and F. N. D. acknowledge CONCYTEC for the two graduate fellowship under Grants No. 233-2015-2-CONCYTEC-FONDECYT and No. 000236-2015-FONDECYT-DE.

We also thank S. Hernández, E. Massoni, and J. Hoefken for useful discussions.

APPENDIX A: SOME PROBABILITY FORMULAS

The dissipative matrix defined by Eq. (4) can be parameterized, in general, by 36 free parameters in the following form:

$$\mathbf{D}=\begin{pmatrix} -\gamma_1 & \beta_{12} & \beta_{13} & \beta_{14} & \beta_{15} & \beta_{16} & \beta_{17} & \beta_{18} \\ \beta_{12} & -\gamma_2 & \beta_{23} & \beta_{24} & \beta_{25} & \beta_{26} & \beta_{27} & \beta_{28} \\ \beta_{13} & \beta_{23} & -\gamma_3 & \beta_{34} & \beta_{35} & \beta_{36} & \beta_{37} & \beta_{38} \\ \beta_{14} & \beta_{24} & \beta_{34} & -\gamma_4 & \beta_{45} & \beta_{46} & \beta_{47} & \beta_{48} \\ \beta_{15} & \beta_{25} & \beta_{35} & \beta_{45} & -\gamma_5 & \beta_{56} & \beta_{57} & \beta_{58} \\ \beta_{16} & \beta_{26} & \beta_{36} & \beta_{46} & \beta_{56} & -\gamma_6 & \beta_{67} & \beta_{68} \\ \beta_{17} & \beta_{27} & \beta_{37} & \beta_{47} & \beta_{57} & \beta_{67} & -\gamma_7 & \beta_{78} \\ \beta_{18} & \beta_{28} & \beta_{38} & \beta_{48} & \beta_{58} & \beta_{68} & \beta_{78} & -\gamma_8 \end{pmatrix}. \tag{A1}$$

However, we will focus on the survival probabilities for only two cases: β_{12} and β_{24}. Below, we display these probabilities:

For β_{12},

$$\begin{aligned} P_{\nu_\alpha\nu_\alpha}=&\frac{1}{3}+\frac{1}{2}\Bigg(((\rho_1^\alpha)^2+(\rho_2^\alpha)^2)\frac{(e^{\Omega_{12}t}+e^{-\Omega_{12}t})}{2} \\ &+((\rho_4^\alpha)^2+(\rho_5^\alpha)^2)\cos\Delta_{13}t+((\rho_6^\alpha)^2+(\rho_7^\alpha)^2)\cos\Delta_{23}t \\ &+(\rho_3^\alpha)^2+(\rho_8^\alpha)^2+\beta_{12}\frac{(e^{\Omega_{12}t}-e^{-\Omega_{12}t})}{\Omega_{12}}\rho_1^\alpha\rho_2^\alpha\Bigg)e^{-\Gamma t}. \end{aligned} \tag{A2}$$

For β_{24},

$$P_{\nu_\alpha\nu_\alpha} = \frac{1}{3} + \frac{e^{-\Gamma t}}{2}\left(\frac{(e^{\Omega_+ t}+e^{-\Omega_+ t})}{2\sqrt{\Omega^4-4\Delta_{12}^2\Delta_{13}^2}}\times g^{-,1}_{+,2} + \frac{(e^{\Omega_- t}+e^{-\Omega_- t})}{2\sqrt{\Omega^4-4\Delta_{12}^2\Delta_{13}^2}} g^{+,1}_{-,2} + \frac{(e^{\Omega_+ t}+e^{-\Omega_+ t})}{2\sqrt{\Omega^4-4\Delta_{12}^2\Delta_{13}^2}} g^{+,4}_{-,5} + \frac{(e^{\Omega_- t}+e^{-\Omega_- t})}{2\sqrt{\Omega^4-4\Delta_{12}^2\Delta_{13}^2}} g^{-,4}_{+,5} + ((\rho_6^\alpha)^2+(\rho_7^\alpha)^2)\cos\Delta_{23}t + (\rho_3^\alpha)^2+(\rho_8^\alpha)^2 + \beta_{24}\frac{1}{\sqrt{\Omega^4-4\Delta_{12}^2\Delta_{13}^2}} \times\left[(\Omega_+(e^{\Omega_+ t}-e^{-\Omega_+ t})-\Omega_-(e^{\Omega_- t}-e^{-\Omega_- t}))\rho_2^\alpha\rho_4^\alpha + \Delta_{12}\Delta_{13}\left(\frac{e^{\Omega_+ t}-e^{-\Omega_+ t}}{\Omega_+}-\frac{e^{\Omega_- t}-e^{-\Omega_- t}}{\Omega_-}\right)\rho_1^\alpha\rho_5^\alpha\right]\right), \tag{A3}$$

where

$$g^{(\pm)_{\rm up},i}_{(\pm)_{\rm down},j} = ((\pm)_{\rm up}(\Delta_{12}^2+\Omega'^2_{(\pm)_{\rm up}})(\rho_i^\alpha)^2 \; (\pm)_{\rm down}(\Delta_{13}^2+\Omega'^2_{(\pm)_{\rm down}})(\rho_j^\alpha)^2),$$

with $\Omega'^2_\pm = \frac{1}{2}(\Omega^2 \pm \sqrt{\Omega^4-4\Delta_{12}^2\Delta_{13}^2})$.

APPENDIX B: CONSTRAINTS FOR THE DECOHERENCE MATRIX ELEMENTS

For the two-flavor and three-flavor cases, the conditions for the decoherence entries can be found in Refs. [27,53], respectively. Here, we display the latter:

$$\begin{aligned}
0 &\le |\vec{a}_1| = -\gamma_1+\gamma_2+\gamma_3-\frac{1}{3}\gamma_8,\\
0 &\le |\vec{a}_2| = \gamma_1-\gamma_2+\gamma_3-\frac{1}{3}\gamma_8,\\
0 &\le |\vec{a}_3| = \gamma_1+\gamma_2-\gamma_3-\frac{1}{3}\gamma_8,\\
0 &\le |\vec{a}_4| = -\gamma_4+\gamma_5+\frac{2}{3}\gamma_8-\frac{2}{\sqrt{3}}\beta_{38},\\
0 &\le |\vec{a}_5| = \gamma_4-\gamma_5+\frac{2}{3}\gamma_8-\frac{2}{\sqrt{3}}\beta_{38},\\
0 &\le |\vec{a}_6| = -\gamma_6+\gamma_7+\frac{2}{3}\gamma_8+\frac{2}{\sqrt{3}}\beta_{38},\\
0 &\le |\vec{a}_7| = \gamma_6-\gamma_7+\frac{2}{3}\gamma_8+\frac{2}{\sqrt{3}}\beta_{38},\\
0 &\le |\vec{a}_8| = -\frac{1}{3}\gamma_1-\frac{1}{3}\gamma_2-\frac{1}{3}\gamma_3+\frac{2}{3}\gamma_4+\frac{2}{3}\gamma_5+\frac{2}{3}\gamma_6+\frac{2}{3}\gamma_7-\gamma_8,
\end{aligned} \tag{B1}$$

with the following Schwartz inequalities:

$$\begin{aligned}
4\beta_{12}{}^2 &\le \left(\gamma_3-\frac{\gamma_8}{3}\right)^2-(\gamma_1-\gamma_2)^2,\\
4\beta_{13}{}^2 &\le \left(\gamma_2-\frac{\gamma_8}{3}\right)^2-(\gamma_1-\gamma_3)^2,\\
4\beta_{23}{}^2 &\le \left(\gamma_1-\frac{\gamma_8}{3}\right)^2-(\gamma_2-\gamma_3)^2,\\
4\beta_{45}{}^2 &\le \left(\frac{2\gamma_8}{3}-\frac{2\beta_{38}}{\sqrt{3}}\right)^2-(\gamma_4-\gamma_5)^2,\\
4\beta_{67}{}^2 &\le \left(\frac{2\gamma_8}{3}+\frac{2\beta_{38}}{\sqrt{3}}\right)^2-(\gamma_6-\gamma_7)^2,\\
\left(\frac{2}{3}\beta_{38}+\frac{1}{\sqrt{3}}\gamma_4+\frac{1}{\sqrt{3}}\gamma_5-\frac{1}{\sqrt{3}}\gamma_6-\frac{1}{\sqrt{3}}\gamma_7\right)^2 &\le |\vec{a}_3||\vec{a}_8|,\\
\left(\frac{1}{\sqrt{3}}\beta_{16}-\frac{1}{\sqrt{3}}\beta_{27}+\frac{1}{\sqrt{3}}\beta_{34}+\frac{5}{3}\beta_{48}\right)^2 &\le |\vec{a}_4||\vec{a}_8|,\\
\left(\frac{1}{\sqrt{3}}\beta_{17}+\frac{1}{\sqrt{3}}\beta_{26}+\frac{1}{\sqrt{3}}\beta_{35}+\frac{5}{3}\beta_{58}\right)^2 &\le |\vec{a}_5||\vec{a}_8|,\\
\left(\frac{1}{\sqrt{3}}\beta_{14}+\frac{1}{\sqrt{3}}\beta_{25}-\frac{1}{\sqrt{3}}\beta_{36}+\frac{5}{3}\beta_{68}\right)^2 &\le |\vec{a}_6||\vec{a}_8|,\\
\left(\frac{1}{\sqrt{3}}\beta_{15}-\frac{1}{\sqrt{3}}\beta_{24}-\frac{1}{\sqrt{3}}\beta_{37}+\frac{5}{3}\beta_{78}\right)^2 &\le |\vec{a}_7||\vec{a}_8|,\\
\left(\beta_{14}-\beta_{25}+\beta_{36}+\frac{1}{\sqrt{3}}\beta_{68}\right)^2 &\le |\vec{a}_1||\vec{a}_4|,\\
\left(\beta_{15}+\beta_{24}+\beta_{37}+\frac{1}{\sqrt{3}}\beta_{78}\right)^2 &\le |\vec{a}_1||\vec{a}_5|,\\
\left(\beta_{16}+\beta_{27}-\beta_{34}+\frac{1}{\sqrt{3}}\beta_{48}\right)^2 &\le |\vec{a}_1||\vec{a}_6|,\\
\left(\beta_{17}-\beta_{26}-\beta_{35}+\frac{1}{\sqrt{3}}\beta_{58}\right)^2 &\le |\vec{a}_1||\vec{a}_7|,\\
\left(\frac{2}{3}\beta_{18}-\frac{2}{\sqrt{3}}\beta_{46}-\frac{2}{\sqrt{3}}\beta_{57}\right)^2 &\le |\vec{a}_1||\vec{a}_8|,\\
\left(\beta_{15}+\beta_{24}-\beta_{37}-\frac{1}{\sqrt{3}}\beta_{78}\right)^2 &\le |\vec{a}_2||\vec{a}_4|,\\
\left(\beta_{14}-\beta_{25}-\beta_{36}-\frac{1}{\sqrt{3}}\beta_{68}\right)^2 &\le |\vec{a}_2||\vec{a}_5|,\\
\left(\beta_{17}-\beta_{26}+\beta_{35}-\frac{1}{\sqrt{3}}\beta_{58}\right)^2 &\le |\vec{a}_2||\vec{a}_6|,\\
\left(\beta_{16}+\beta_{27}+\beta_{34}-\frac{1}{\sqrt{3}}\beta_{48}\right)^2 &\le |\vec{a}_2||\vec{a}_7|,\\
\left(\frac{2}{3}\beta_{28}+\frac{2}{\sqrt{3}}\beta_{47}-\frac{2}{\sqrt{3}}\beta_{56}\right)^2 &\le |\vec{a}_2||\vec{a}_8|,\\
\left(\beta_{16}-\beta_{27}-\beta_{34}-\frac{1}{\sqrt{3}}\beta_{48}\right)^2 &\le |\vec{a}_3||\vec{a}_4|,
\end{aligned}$$

$$\left(\beta_{17}+\beta_{26}-\beta_{35}-\frac{1}{\sqrt{3}}\beta_{58}\right)^2 \le |\vec{a}_3||\vec{a}_5|,$$
$$\left(\beta_{14}+\beta_{25}+\beta_{36}-\frac{1}{\sqrt{3}}\beta_{68}\right)^2 \le |\vec{a}_3||\vec{a}_6|,$$
$$\left(\beta_{15}-\beta_{24}+\beta_{37}-\frac{1}{\sqrt{3}}\beta_{78}\right)^2 \le |\vec{a}_3||\vec{a}_7|,$$
$$\left(\beta_{46}-\beta_{57}-\frac{2}{\sqrt{3}}\beta_{18}\right)^2 \le |\vec{a}_4||\vec{a}_6|,$$
$$\left(\beta_{47}+\beta_{56}+\frac{2}{\sqrt{3}}\beta_{28}\right)^2 \le |\vec{a}_4||\vec{a}_7|,$$
$$\left(\beta_{47}+\beta_{56}-\frac{2}{\sqrt{3}}\beta_{28}\right)^2 \le |\vec{a}_5||\vec{a}_6|,$$
$$\left(\beta_{46}-\beta_{57}+\frac{2}{\sqrt{3}}\beta_{18}\right)^2 \le |\vec{a}_5||\vec{a}_7|. \tag{B2}$$

Moreover, in order to analyze the positivity for the matrix $\mathbf{A}$, we use for simplicity our optimal case, composed by β_{12}, β_{28}, β_{56}, and β_{47}:

$$\mathbf{D}=\begin{pmatrix} -\Gamma & \beta_{12} & 0 & 0 & 0 & 0 & 0 & 0 \\ \beta_{12} & -\Gamma & 0 & 0 & 0 & 0 & 0 & \beta_{28} \\ 0 & 0 & -\Gamma & 0 & 0 & 0 & 0 & 0 \\ 0 & 0 & 0 & -\Gamma & 0 & 0 & \beta_{47} & 0 \\ 0 & 0 & 0 & 0 & -\Gamma & \beta_{56} & 0 & 0 \\ 0 & 0 & 0 & 0 & \beta_{56} & -\Gamma & 0 & 0 \\ 0 & 0 & 0 & \beta_{47} & 0 & 0 & -\Gamma & 0 \\ 0 & \beta_{28} & 0 & 0 & 0 & 0 & 0 & -\Gamma \end{pmatrix}. \tag{B3}$$

Then, the matrix $\mathbf{A}\equiv[a_{kj}]$ is

$$\mathbf{A}=\begin{pmatrix} -\Gamma' & \beta'_{12} & 0 & 0 & 0 & 0 & 0 & 0 \\ \beta'_{12} & -\Gamma' & 0 & 0 & 0 & 0 & 0 & \beta'_{28} \\ 0 & 0 & -\Gamma' & 0 & 0 & 0 & 0 & 0 \\ 0 & 0 & 0 & -\Gamma' & 0 & 0 & \beta'_{47} & 0 \\ 0 & 0 & 0 & 0 & -\Gamma' & \beta'_{56} & 0 & 0 \\ 0 & 0 & 0 & 0 & \beta'_{56} & -\Gamma' & 0 & 0 \\ 0 & 0 & 0 & \beta'_{47} & 0 & 0 & -\Gamma' & 0 \\ 0 & \beta'_{28} & 0 & 0 & 0 & 0 & 0 & -\Gamma' \end{pmatrix}, \tag{B4}$$

with

$$\Gamma'=-\frac{2}{3}\Gamma, \qquad \beta'_{12}=2\beta_{12},$$
$$\beta'_{28}=\frac{2}{3}(\beta_{28}+\sqrt{3}(\beta_{47}-\beta_{56})),$$
$$\beta'_{56}=\beta_{47}+\beta_{56}-\frac{2}{\sqrt{3}}\beta_{28},$$
$$\beta'_{47}=\beta_{47}+\beta_{56}+\frac{2}{\sqrt{3}}\beta_{28}. \tag{B5}$$

We get its corresponding eigenvalues:

$$\lambda_{1,2}=\frac{2}{3}\Gamma\ge 0,$$
$$\lambda_{3,4}=\frac{1}{3}(2\Gamma-3(\beta_{47}+\beta_{56})\mp 2\sqrt{3}\beta_{28})\ge 0,$$
$$\lambda_{5,6}=\frac{1}{3}(2\Gamma+3(\beta_{47}+\beta_{56})\mp 2\sqrt{3}\beta_{28})\ge 0,$$
$$\lambda_{7,8}=\frac{2}{3}(\Gamma\mp(9\beta_{12}^2+\beta_{28}^2+3(\beta_{47}^2+\beta_{56}^2) +2\sqrt{3}\beta_{28}(\beta_{47}-\beta_{56})-6\beta_{47}\beta_{56})^{1/2})\ge 0. \tag{B6}$$

Thus, using Eqs. (B6) and (B2), we can obtain the following individual maximum values for said β's: $|\beta_{28}|=1/\sqrt{3}$, $|\beta_{12}|=1/3$, $|\beta_{56}|=1/\sqrt{3}$, and $|\beta_{47}|=1/\sqrt{3}$. When we set all the aforementioned β's together and follow the procedure described in Sec. II B 5, we get afterwards $\beta_{28}=\Gamma/\sqrt{3}$, $\beta_{12}=(\sqrt{2/3})\Gamma/3$, and $\beta_{56}=-\beta_{47}=\Gamma/3$.

[1] S. Fukuda *et al.* (Super-Kamiokande Collaboration), Phys. Rev. Lett. **86**, 5651 (2001).
[2] Q. R. Ahmad *et al.* (SNO Collaboration), Phys. Rev. Lett. **89**, 011302 (2002).
[3] Y. Fukuda *et al.* (Super-Kamiokande Collaboration), Phys. Rev. Lett. **81**, 1562 (1998).
[4] T. Kajita, E. Kearns, and M. Shiozawa (Super-Kamiokande Collaboration), Nucl. Phys. **B908**, 14 (2016).
[5] T. Araki *et al.* (KamLAND Collaboration), Phys. Rev. Lett. **94**, 081801 (2005).
[6] F. P. An *et al.* (Daya Bay Collaboration), Phys. Rev. Lett. **108**, 171803 (2012).
[7] P. Adamson *et al.* (MINOS Collaboration), Phys. Rev. D **77**, 072002 (2008).
[8] J. K. Ahn, S. Chebotaryov, J. H. Choi, S. Choi, W. Choi, Y. Choi, H. I. Jang, J. S. Jang, E. J. Jeon, I. S. Jeong *et al.* (RENO Collaboration), Phys. Rev. Lett. **108**, 191802 (2012).
[9] Y. Abe *et al.* (Double CHOOZ Collaboration), Phys. Rev. Lett. **108**, 131801 (2012).
[10] A. B. McDonald *et al.* (SNO Collaboration), Phys. Scr. T **T121**, 29 (2005).
[11] M. Gasperini, Phys. Rev. D **38**, 2635 (1988).
[12] A. Halprin and C. N. Leung, Phys. Rev. Lett. **67**, 1833 (1991).
[13] A. M. Gago, H. Nunokawa, and R. Zukanovich Funchal, Phys. Rev. Lett. **84**, 4035 (2000).
[14] D. Colladay and V. A. Kostelecky, Phys. Rev. D **55**, 6760 (1997).
[15] S. R. Coleman and S. L. Glashow, Phys. Rev. D **59**, 116008 (1999).
[16] S. R. Coleman and S. L. Glashow, Phys. Lett. B **405**, 249 (1997).
[17] D. Colladay and V. A. Kostelecky, Phys. Rev. D **58**, 116002 (1998).
[18] P. Adamson *et al.* (MINOS Collaboration), Phys. Rev. Lett. **101**, 151601 (2008).
[19] P. Adamson *et al.* (MINOS Collaboration), Phys. Rev. Lett. **105**, 151601 (2010).
[20] A. A. Aguilar-Arevalo *et al.* (MiniBooNE Collaboration), Phys. Lett. B **718**, 1303 (2013).
[21] Y. F. Li and Z. H. Zhao, Phys. Rev. D **90**, 113014 (2014).
[22] M. Jacobson and T. Ohlsson, Phys. Rev. D **69**, 013003 (2004).
[23] J. Ellis, N. E. Mavromatos, and D. V. Nanopoulos, Phys. Lett. B **293**, 37 (1992); Int. J. Mod. Phys. A **11**, 1489 (1996).
[24] F. Benatti and R. Floreanini, Ann. Phys. (N.Y.) **273**, 58 (1999).
[25] S. W. Hawking, Commun. Math. Phys. **87**, 395 (1982); Phys. Rev. D **37**, 904 (1988); **53**, 3099 (1996); S. W. Hawking and C. J. Hunter, Phys. Rev. D **59**, 044025 (1999).
[26] F. Benatti and R. Floreanini, J. High Energy Phys. 02 (2000) 032.
[27] F. Benatti and R. Floreanini, Phys. Rev. D **64**, 085015 (2001).
[28] E. Lisi, A. Marrone, and D. Montanino, Phys. Rev. Lett. **85**, 1166 (2000).
[29] A. M. Gago, E. M. Santos, W. J. C. Teves, and R. Zukanovich Funchal, Phys. Rev. D **63**, 073001 (2001).
[30] A. M. Gago, E. M. Santos, W. J. C. Teves, and R. Zukanovich Funchal, arXiv:hep-ph/0208166.
[31] G. Barenboim and N. E. Mavromatos, J. High Energy Phys. 01 (2005) 034.
[32] G. L. Fogli, E. Lisi, A. Marrone, D. Montanino, and A. Palazzo, Phys. Rev. D **76**, 033006 (2007).
[33] Y. Farzan, T. Schwetz, and A. Y. Smirnov, J. High Energy Phys. 07 (2008) 067.
[34] R. L. N. Oliveira and M. M. Guzzo, Eur. Phys. J. C **73**, 2434 (2013).
[35] J. A. Carpio, E. Massoni, and A. M. Gago, Phys. Rev. D **97**, 115017 (2018).
[36] R. M. Wald, Phys. Rev. D **21**, 2742 (1980).
[37] N. E. Mavromatos, J. Phys. Conf. Ser. **171**, 012007 (2009).
[38] Y. Liu, L. Hu, and M. L. Ge, Phys. Rev. D **56**, 6648 (1997).
[39] J. Ellis, J. L. Lopez, N. E. Mavromatos, and D. V. Nanopoulos, Phys. Rev. D **53**, 3846 (1996); J. Ellis, N. E. Mavromatos, and D. V. Nanopoulos, Phys. Rev. D **63**, 024024 (2000).
[40] R. Acciarri *et al.* (DUNE Collaboration), arXiv:1512.06148.
[41] T. Alion *et al.* (DUNE Collaboration), arXiv:1606.09550.
[42] B. Pontecorvo, Zh. Eksp. Teor. Fiz. **33**, 549 (1957) [Sov. Phys. JETP **6**, 429 (1957)].
[43] Z. Maki, M. Nakagawa, and S. Sakata, Prog. Theor. Phys. **28**, 870 (1962).
[44] http://www.nu-fit.org.
[45] M. V. Ascencio-Sosa, A. M. Calatayud-Cadenillas, A. M. Gago, and J. Jones-Pérez, Eur. Phys. J. C **78**, 809 (2018).
[46] M. Masud, M. Bishai, and P. Mehta, Sci. Rep. **9**, 352 (2019).
[47] J. M. Berryman, A. de Gouvea, K. J. Kelly, and A. Kobach, Phys. Rev. D **92**, 073012 (2015).
[48] P. Huber, M. Lindner, and W. Winter, Comput. Phys. Commun. **167**, 195 (2005).
[49] P. Huber, J. Kopp, M. Lindner, M. Rolinec, and W. Winter, Comput. Phys. Commun. **177**, 432 (2007).
[50] C. A. Argüelles Delgado, J. Salvado, and C. N. Weaver, Comput. Phys. Commun. **196**, 569 (2015).
[51] D. Indumathi and N. Sinha, Phys. Rev. D **80**, 113012 (2009).
[52] A. Donini, J. J. Gomez Cadenas, and D. Meloni, J. High Energy Phys. 02 (2011) 095.
[53] S. Hernández, Master's thesis, Pontificia Universidad Católica del Perú, 2016.